COBEM 2023 27TH INTERNATIONAL CONGRESS OF MECHANICAL ENGENEERING

ABCM Brazilian Society of Mechanical Sciences and Engineering
27th ABCM International Congress of Mechanical Engineering
December 04-08, 2023, Florianópolis-SC, Brazil

# COB-2023-1460
# EXPERIMENTAL THERMAL PERFORMANCE EVALUATION OF AN AUTOMOTIVE AIR CONDITIONING SYSTEM

**Diogo Lôndero da Silva**
**Igor Santos de Oliveira**
**Aline Durrer Patelli Juliani**
ReVe - Vehicular Refrigeration Laboratory, Mobility Engineering Department, Federal University of Santa Catarina, Joinville, SC, Brazil, diogo.londero@ufsc.br

**Filipe Fischer**
Techsolution Ltda, Product Development Engineering, São José dos Pinhais, PR, Brazil.

**Guilherme Medeiros de Cordova**
Renault do Brasil SA, Product Development Engineering - RTA, São José dos Pinhais, PR, Brazil.

***Abstract.*** *Brazil is considered one of the largest passenger car producers of the world and is at the top of this ranking in South America. Among the different functional requirements related to a passenger car design, the thermal comfort stands out, especially in tropical/subtropical countries like Brazil. Despite its benefits, the operation of an air conditioning system not only increases the fuel consumption of the vehicle, but also puts the greenhouse gas emissions up. In addition, the new platform of electric vehicles (EVs), which has progressively attracted the attention of the scientific and industrial community, also presents technological challenges related to air conditioning, since its operation can reduce driving range. Therefore, the aim of this paper is to build an experimental apparatus to evaluate the energy efficiency of an automotive air conditioning system based on the first and second laws of thermodynamics. While conducting the experiments, the compressor rotational speed and the evaporator air mass flow rate were considered as independent variables. The experimental results were analyzed considering the fundamentals of thermodynamics to quantify cooling capacity, power consumption and the irreversibilities associated with each component of the air conditioning system. The results showed that the average COP of the system is reduced by increasing the compressor rotation speed or reducing the evaporator airflow. In addition, a second law analysis showed that the compressor accounts for 84% of the irreversibility in the system, while the condenser is responsible for 9%.*

***Keywords:*** *Automotive air conditioning, Experimental work, Energy efficiency*

## 1. INTRODUCTION

Brazil is among the 10th largest passenger car producers of the world and is at the top of this ranking in South America. According to ANFAVEA (2023), since 2016, the annual production of light cars, which includes passenger cars and light commercial vehicles, is around two million units. For this class of vehicles, it is noticed that thermal comfort is a crucial functional requirement, particularly in tropical/subtropical countries like Brazil (Torregrosa-Jaime *et al*., 2015). Consequently, in 2022, the introduction of new launches and model updates made air conditioning systems a standard feature, resulting in 100% of the new cars manufactured in Brazil being equipped with an air conditioning system. (Motor, 2022).

In general, the climate control system is the main auxiliary load in a passenger car and its use not only raises fuel/energy consumption, but also increases the direct and indirect greenhouse gas emissions (Farrington and Rugh, 2000; Da Silva and Melo, 2016). Due to the impact on global warming caused using R-134a, the automotive industry has sought new options of refrigerants that can be used both in vehicles equipped with internal combustion engines or electric motors. Furthermore, the Kigali Amendment, initiated in 2019, sets a target to gradually reduce HFCs (hydrofluorocarbons) by 80-85% by 2050. Currently, among the main options to replace R-134a (GWP 1430) in the automotive industry, there are R-744, R-1234yf and R-152a, which have GWP equal to 1, 4 and 124, respectively (Bandarra and Mendonza, 2010; Unep, 2023).

The energy consumption of an automotive air conditioning system, responsible for an average increase in the fuel consumption ranging from 3% up to 20%, depends on several factors such as driving and whether condition, vehicle type, efficiency of the A/C components and number of passengers (IEA, 2019; Jabardo *et al*., 2002; Da Silva *et al*., 2019). Johnson (2002) estimated that the use of vehicular air conditioning systems is responsible for 6% of the USA crude oil consumption, which corresponds to 27 billion liters of gasoline per year. Additionally, it is observed that the use of the A/C system in electric vehicles (EVs), especially in the heating mode, requires the use of more efficient concepts to

compensate for the lower driving range of this technology, when compared to vehicles equipped with internal combustion engines (Wu *et al*., 2020; Zhang *et al*., 2020).

Due to these facts, the energy consumption of automotive A/C systems has gained significant attention from industry, academia, and regulatory agencies. For instance, Da Silva and Cordova (2017) proposed a mathematical model for an automotive air conditioning system to predict the thermal performance of the system, considering different operating conditions and charge of fluid refrigerant. Comparing the performance of different refrigerants, Kuwar and Narasimham (2020) observed a reduction of 2 - 5% on the COP by replacing R-134a by R-1234yf. In a different study, Ko *et al*. (2021) created a transient model to examine energy consumption during the pull-down time. They found that the initial temperature of the vehicle cabin has a noteworthy impact on energy consumption. More recently, Caron *et al*. (2022) put forward a first principle model to simulate the thermal performance of the A/C system of a hybrid vehicle equipped with microchannel heat exchangers, observing an inverse relation between COP and the compressor speed.

The literature review shows that identifying opportunities to improve the thermodynamic performance of the automotive air conditioning systems or the development of mathematical models relies on experimental measurements of the key performance indicators of the system such as the thermodynamic state of the fluid refrigerant at distinct locations of the system, cooling capacity and energy consumption. Therefore, the objective of this paper is to construct an experimental apparatus that enables the energy performance assessment of an automotive air conditioning system and its components through practical experiments and thermodynamic principles.

## 2. EXPERIMENTAL FACILITY

The experimental facility consists of the air conditioning system components used in a typical five-passenger car, equipped with additional transducers used to measure the power consumption and the air and fluid refrigerant properties at distinct positions of the system. For this work, the performance of the individual components and the system has been investigated considering two major independent variables, namely the compressor speed and the airflow rate at the evaporator.

### 2.1 Refrigeration circuit description

Figure 1 shows the experimental apparatus and the corresponding refrigeration circuit. The experimental apparatus depicted in Fig. 1a is equipped with a fixed-displacement reciprocating compressor, a thermostatic expansion valve externally equalized and two heat exchangers. The condenser employs a microchannel heat exchanger design, while the evaporator utilizes an aluminum plate concept. A variable velocity electric motor is used to drive the compressor, allowing the control of the compressor rotational speed. Rubber hoses and aluminum alloy pipes are used to connect the components. The fluid refrigerant and lubricant oil are R-134a and PAG (Polyalkylene glycol), respectively.

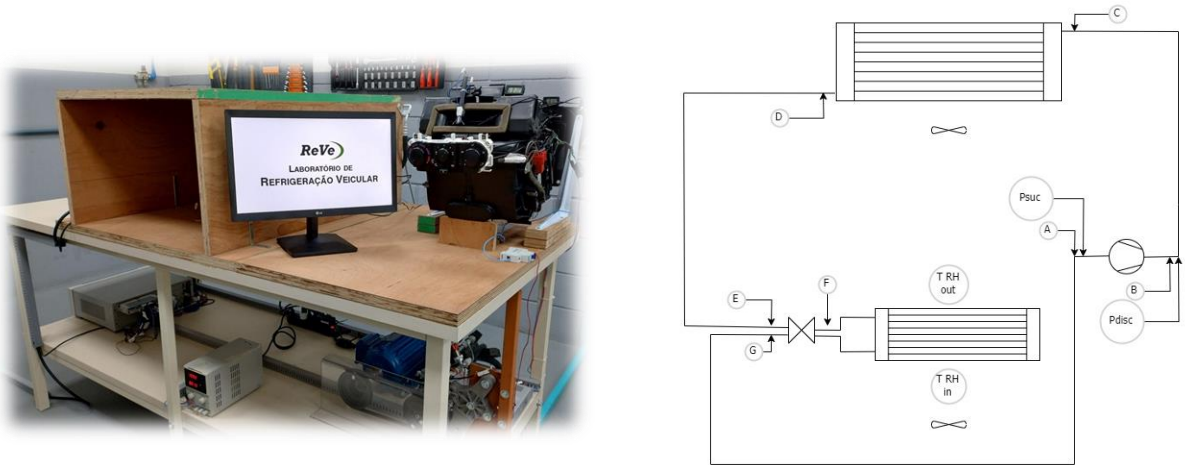


(a) (b)

Figure 1. Experimental apparatus (a) and schematic representation of the refrigeration circuit (b).

Figure 1b shows that the refrigeration cycle starts with the compression process (A→B), in which the temperature of the refrigerant vapor is raised above the surrounding temperature. The superheated refrigerant, leaving the compressor is pre-cooled (B→C) in the discharge line, and passes through the condenser where it releases heat to the surroundings and changes for a liquid state (C→D). The subcooled high-pressure liquid is stored in a receiver-dryer attached to the

condenser that allows only liquid refrigerant to reach the inlet of the thermostatic expansion valve. The liquid refrigerant then undergoes an expansion process through the thermostatic valve (E→F), which controls the mass flow rate based on the measured refrigerant superheat at the evaporator outlet position. Subsequently, the two-phase low-pressure refrigerant, from the outlet of the thermostatic expansion valve, flows through the evaporator (F→G) to exchange heat with the external airflow and returns to the compressor suction line (G→A), completing the cycle. As the ambient air passes through the evaporator, its temperature and humidity decrease. Thus, the cold and dry air produced is ready to be supplied.

The evaporator, the fan (blower) and the expansion valve are housed in a Heating Ventilation and Air Conditioning (HVAC) unit, presented in Fig. 2. During normal operation, the HVAC unit is assembled inside the vehicle dashboard, not being visible to the passengers of a vehicle. The positions where the evaporator and the blower are mounted in the HVAC unit are highlighted in Fig. 2a by the blue and yellow colors, respectively. Additionally, in Fig. 2b, a schematic depiction illustrates the internal airflow within the HVAC unit. As can be seen in Fig. 2b, the external air (1) is suctioned by the fan (2) and forced against the evaporator (3) indicated in blue. The second heat exchanger, depicted in red, is activated when the heating mode is required. After the air being cooled and dehumidified by the evaporator, it is blown into the passenger's cabin (4). Dampers, indicated by D letter in Fig. 2b, are employed to change the airflow in various directions, such as the windshield or the floor of the vehicle. The HVAC unit is also equipped with a filter and allows the air inside the cabin to be recirculated through the heat exchangers, without considerable admission of external fresh air (1). In this study, the HVAC unit was tested as presented in Fig. 1a, the heating mode was not considered and the dampers were adjusted to suction and supply air by positions 1 and 4 of Fig. 2b, respectively.

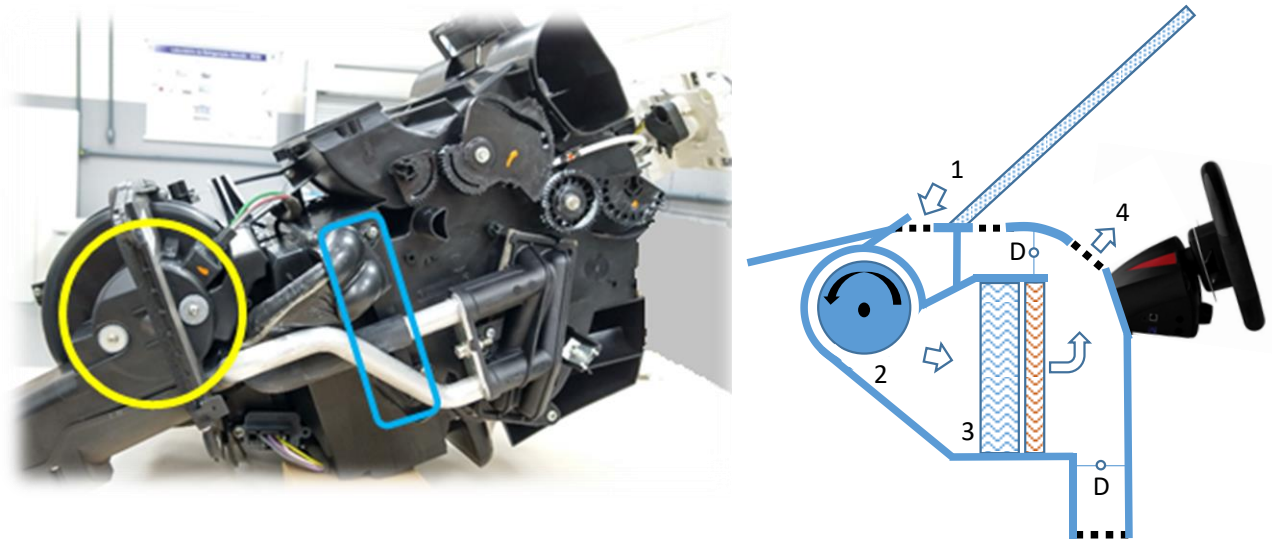


(a) (b)

Figure 2. HVAC unit (a) and its schematic representation

## 2.2 Measurement system description

The thermodynamic properties of the air and the fluid refrigerant were determined based on the measurements of temperature, pressure and relative humidity at distinct positions of the test rig, as indicated in Fig. 1b. The temperature was measured using T type thermocouples, while the refrigerant pressure using absolute pressure transducers with uncertainties of ±0.5°C and ±0.2 bar, respectively. The relative humidity was measured at both the inlet and outlet positions of the evaporator, with uncertainty of ±2%. The fluid refrigerant temperature was measured at the external surface of the tubes, while the refrigerant pressure was measured at the suction and discharge lines of the compressor. Figure 3a shows the refrigerant temperature transducer installed at the surface of a pipe located at the condenser inlet, while Fig. 3b depicts two valves at the top of the compressor, where the pressure transducers were installed to measure the refrigerant pressure.

The compressor rotation speed was measured with an optical tachometer providing an uncertainty of ±1 rpm, while the power consumption of the compressor was calculated based on the power supplied by the electric motor to the shaft of the pulley, taking into account the efficiency of the pulley-belt transmission system. The shaft power was continuously measured by the frequency inverter of the motor with uncertainty of ±1 W. Average air velocities at evaporator and condenser were also measured using a handheld anemometer with a maximum uncertainty of ±0.05 m/s.

(a) (b)

Figure 3. Temperature transducer (a) and compressor pulley-belt transmission system (b)

## 3. EXPERIMENTAL DATA ANALYSIS

The experimental data of the air conditioning system was analyzed under steady conditions. The first law of thermodynamics, without the kinetic and potential energies terms, expressed by

$$\dot{Q} + \dot{W} + \sum \dot{m}_{in}\, h_{in} - \sum \dot{m}_{out}\, h_{out} = 0 \tag{1}$$

was applied on the main components of the air conditioning system, where $\dot{Q}$ and $\dot{W}$ are the heat and work rate over the control volume boundaries, $\dot{m}$ represents the mass flow rate and *h* is the enthalpy.

In order to evaluate the irreversibility related to friction, thermodynamic losses and heat transfer on each component, the second law analysis represented by

$$\sum \dot{m}_{in}\, s_{in} - \sum \dot{m}_{out}\, s_{out} + \sum \frac{\dot{Q}_{sen}}{T} + \frac{R}{MM} \sum \frac{\dot{Q}_{lat}}{L} + \dot{S}_{gen} = 0 \tag{2}$$

was applied, where *s* represents the entropy, *R* is universal gas constant, *MM* is water molecular mass, $\dot{S}_{gen}$ is the entropy generation rate, *T* is absolute temperature measured at the control volume surface subject to heat transfer and *L* is the water vapor latent heat of condensation.

Moreover, the cooling capacity of the evaporator was evaluated as

$$\dot{Q}_e = \dot{m}_{air}\left(h_{a,in} - h_{a,out}\right) \tag{3}$$

were $\dot{m}_{air}$ is the air mass flow rate and $h_a$ represents the enthalpy of the moist air, allowing the evaluation of the coefficient of performance expressed by

$$COP = \frac{\dot{Q}_e}{\dot{W}} \tag{4}$$

in which $\dot{W}$ represents the compressor power consumption.

## 4. RESULTS

Table 1 shows the steady experimental results for different compressor speeds and evaporator airflow rates. During the experiments, the psychrometric state of the air at the evaporator and the condenser inlets were maintained constant. The refrigeration cycle in a pressure-enthalpy diagram, related to test number 2, is presented in Fig. 2. The letters on the diagram correspond to the positions depicted in Fig. 1b. Points A and G of the diagram shows that the fluid refrigerant is superheated at the evaporator outlet and the compressor suction line, while points D and E indicate subcooling at the condenser outlet and the inlet of the expansion valve. Moreover, it is observed that the real compression process occurs remarkably close to the path indicated by the isentropic dashed line. This is mainly justified by the heat rejected by the compressor surface to the surroundings. Although the fluid refrigerant pressure drop in the heat exchangers is not

represented in the p-h diagram, it is considered in the experimental results, adding thermodynamic losses to the performance of the system under analysis. Similar refrigeration cycles were observed in the other operating conditions presented in Tab. 1.

Table 1. Experimental results of the air conditioning system.

| Test | Speed [rpm] | $m_{a,evap}$ [kg/s] | $T_{amb}$ [°C] | $RH_{amb}$ [%] | $P_e$ [bar] | $P_c$ [bar] | $Q_e$ [W] | W [W] | COP |
|---|---|---|---|---|---|---|---|---|---|
| 1 | 500 | 0.058 | 23.0 | 55.0 | 3.50 | 8.55 | 1195 | 572.0 | 2.09 |
| 2 | 680 | 0.058 | 23.0 | 55.0 | 3.30 | 9.45 | 1354 | 789.5 | 1.72 |
| 3 | 890 | 0.037 | 23.0 | 55.0 | 2.90 | 10.00 | 1203 | 1021.0 | 1.18 |
| 4 | 890 | 0.058 | 23.0 | 55.0 | 3.15 | 10.35 | 1442 | 1049.1 | 1.37 |

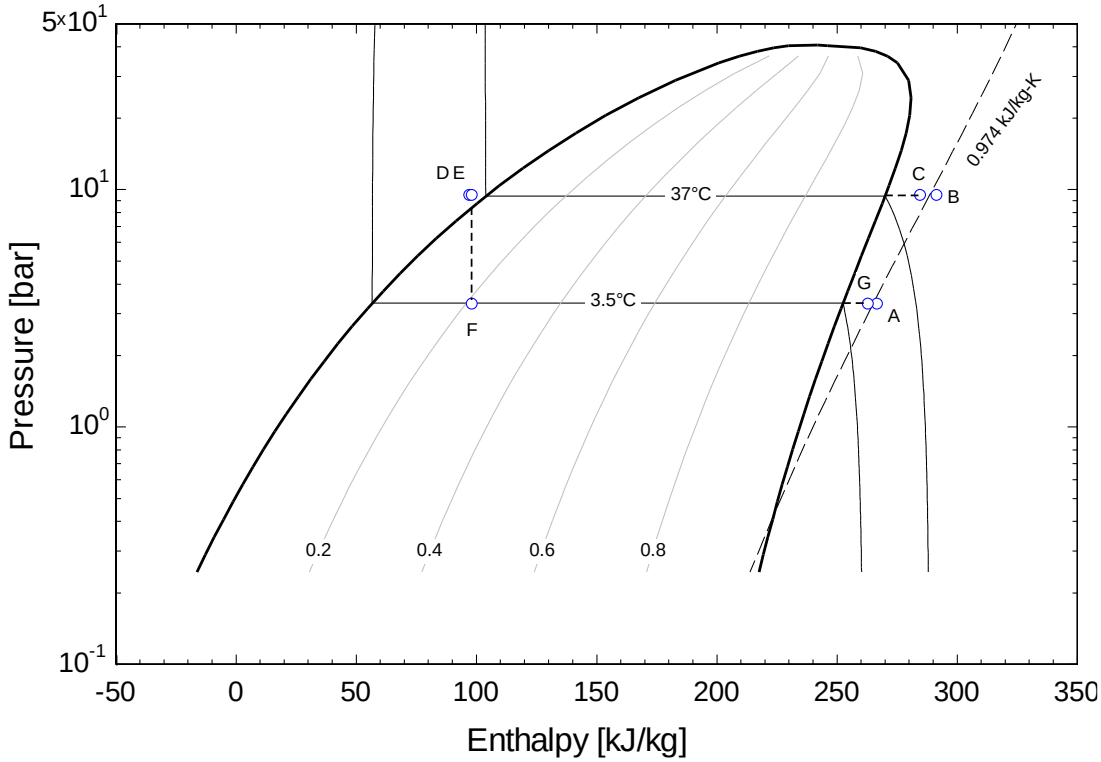


Figure 4. Pressure-Enthalpy diagram of the refrigeration cycle

Figure 5 shows suction and discharge lines pressure evolution for different compressor speeds, being the speed indicated by the dashed line on the right axis of the abscissa. It is observed that increasing the compressor velocity leads to a rise in the pressure ratio ($P_c/P_e$), represented by the distance between the discharge line and suction pressures results. For instance, at 20 minutes, when the compressor speed is increased from 500 to 680 rpm the pressure ratio is increased from 2.4 to a new steady condition of 2.9 at 35 min, which have a simultaneous impact on the condenser and evaporator saturation temperatures, which in turn are depicted in Fig. 6. This behavior is attributed to the search for a new operating condition where the compressor refrigerant mass flow matches that of the expansion valve. It is also observed in Fig. 6 that the evaporation temperature remained above 0°C during all experiments, which is desired in air conditioning applications to avoid the evaporator airflow blockage by frost formation (Hermes *et al.*, 2021). Moreover, the effect of the evaporator airflow rate is observed at times equal to 28 and 48 minutes, in Fig. 5 and Fig 6. As can be seen in Fig. 5, the increase of the evaporator airflow results in a simultaneous increase of suction and discharge pressures, due to the raise of the evaporator thermal load.

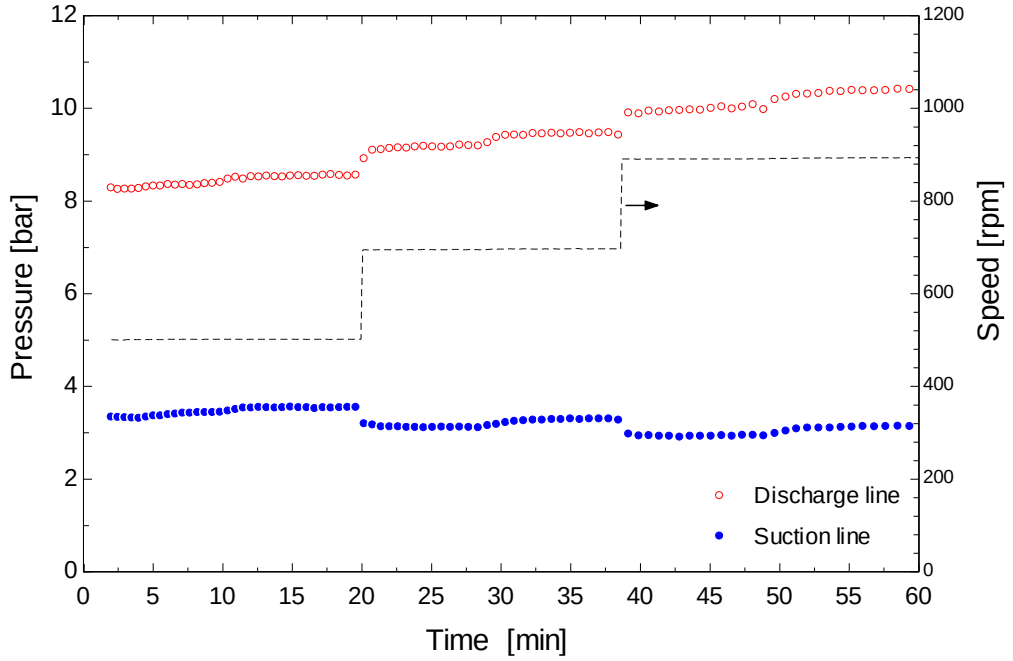


Figure 5. Evolution of pressure of suction and discharge lines for different compressor speeds

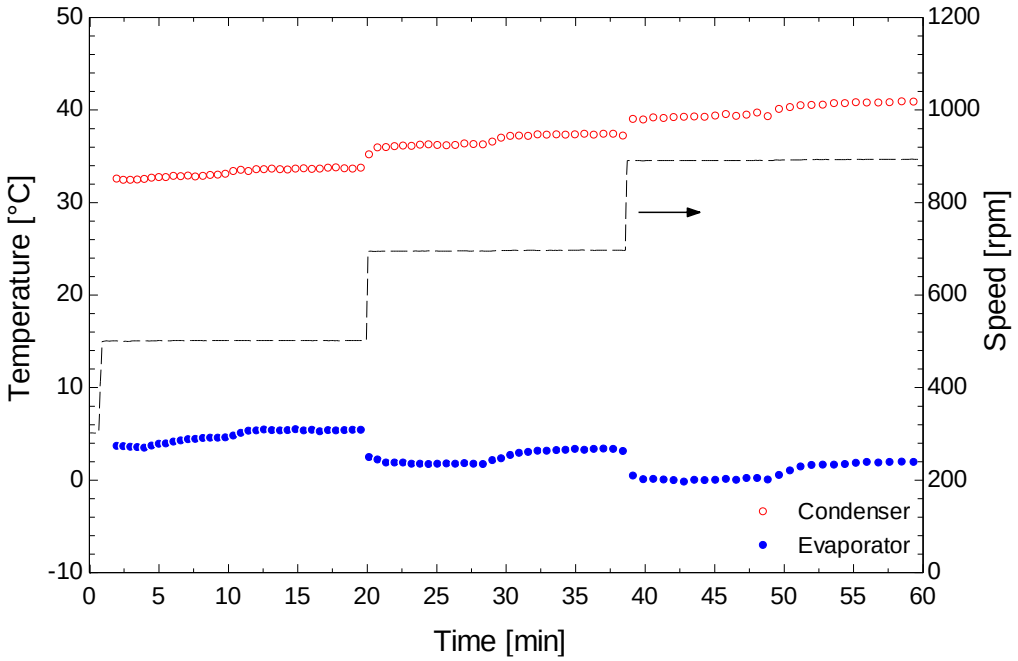


Figure 6. Evolution of saturation temperatures of condenser and evaporator for different compressor speeds

In Figure 7, the cooling capacity of the air conditioning system is compared across different operating conditions described in Table 1. It illustrates the proportion of sensible and latent heat, showing very close values between these two parcels of the total cooling capacity, indicating a sensible heat factor (SHF) close to 0.5 for all conditions. The comparisons of the investigated conditions show that the total cooling capacity increases with the compressor speed and the evaporator air mass flow rate. For instance, the increase of the compressor speed from 500 to 680 rpm (tests 1 and 2) and the evaporator airflow rate from 0.037 to 0.058 kg/s (tests 3 and 4) result in total cooling increases of 13.3% and 19.8%, respectively. When comparing conditions 2 and 3, it is also observed that the increase in compressor speed from 680 to 890 rpm is not able to compensate the reduction in airflow in the evaporator, resulting in a reduction of the cooling capacity from 1354 W to 1203 W. Additionally, it can be seen from Fig. 5 that the change between conditions 2 and 3 occurs approximately after 38 minutes, indicating that the evaporation pressure suffers a reduction. Such a pressure

reduction results in a drop in the density of the fluid refrigerant at the compressor suction port, which in turn compromises the system cooling capacity.

Figure 8 shows the effects of compressor speed and evaporator air mass flow rate on the COP. As can be seen, the reduction of COP observed in conditions 1, 2 and 4 shows that the cooling capacity increase obtained by the compressor rotation change is not adequately balanced by the power consumption increase, leading to an overall decrease in the system's COP, within the investigated experimental domain. On the other hand, the COP presented an increase of 16% (test 3 and 4) due to the evaporator air mass flow rate change, showing that in this scenario the rise in power consumption from 1021 W to 1049 W is offset by the corresponding increase in cooling capacity.

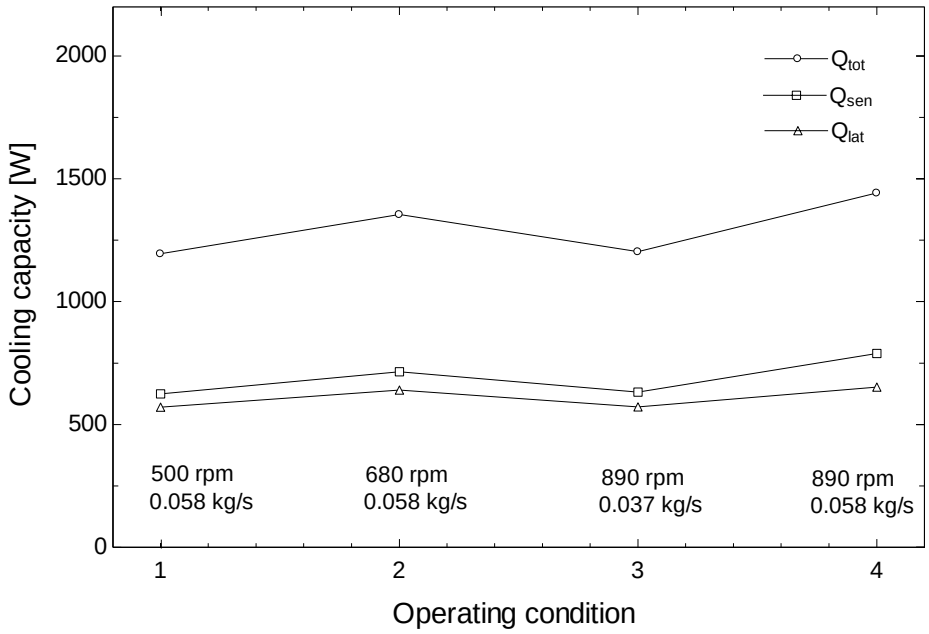


Figure 7. Evaporator cooling capacity for different operating conditions

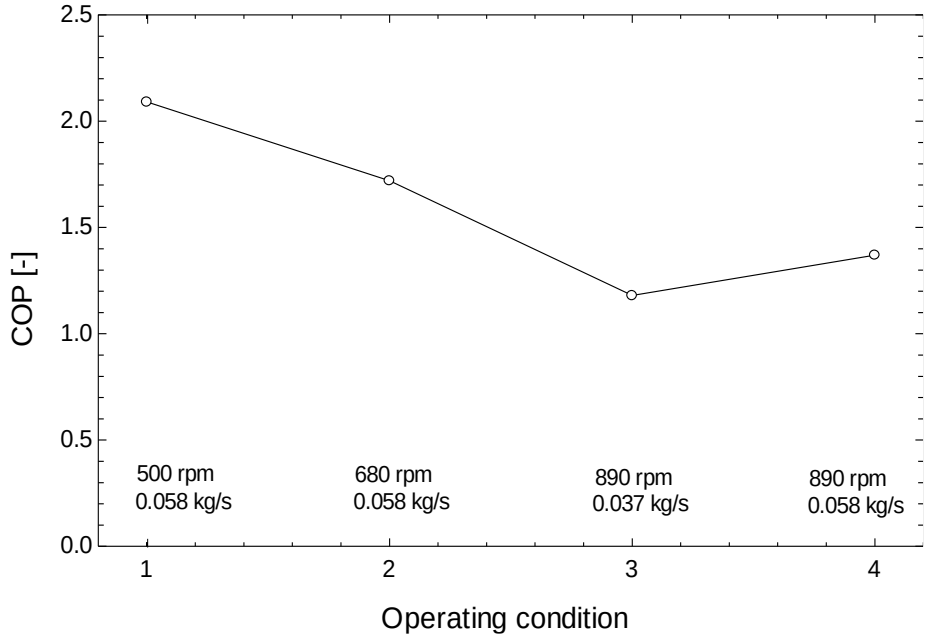


Figure 8. Evaporator cooling capacity for different operating conditions

Figure 9 compares the entropy generation rate evaluated by Eq. 2 for different operating conditions and components of the air conditioning system. It is observed that the increase of the compressor speed and the evaporator air mass flow rate resulted in augmentation of the entropy generation rate. In addition, the results show that, for all the operating conditions, the compressor is the main source of the irreversibilities, followed by the condenser. Comparing the average values among the four operational conditions, it is verified that the compressor and the condenser are responsible for 84% and 9% of the irreversibilities of the system, respectively. These findings indicate that the initial focus for improving the system's energy efficiency should be on redesigning these two components.

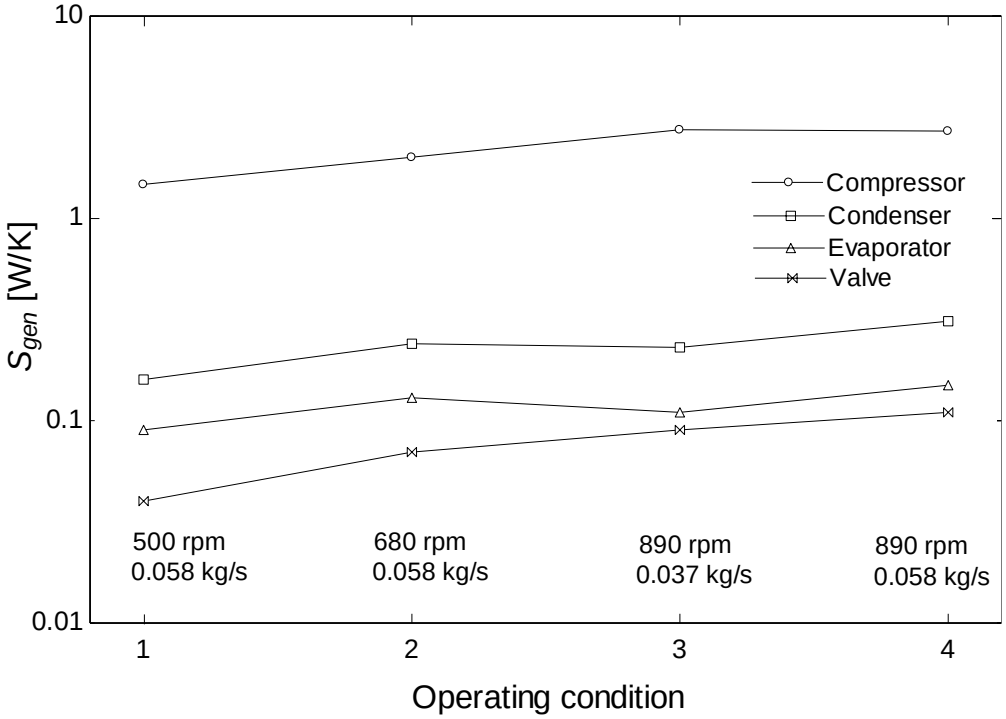


Figure 9. Entropy generation rate for different operating conditions and components of the air conditioning system

## 5. CONCLUSIONS

In this work, an experimental apparatus was designed and built in order to evaluate the energy performance of a typical air conditioning system used in a five-seat passenger vehicle. The experimental results were analyzed based on the first and second laws of thermodynamics. The experimental independent variables were compressor rotational speed and air mass flow rate at the evaporator. Considering the obtained results, certain conclusions can be drawn regarding the system performance and the proposed method:

- The real compression process occurs remarkably close to the path indicated by an isentropic line, which is justified by the heat rejected by the compressor to the surroundings.
- The rise of cooling capacity by the compressor speed is not offset by the power consumption, leading to a decrease in the system's COP.
- On the other hand, the increase of the evaporator air mass flow rate has slightly improved the system's COP.
- The utilized method has demonstrated its effectiveness in prioritizing the components that hold the highest potential for enhancing the energy efficiency of the air conditioning system.
- The second law analysis showed that the compressor is the main source of irreversibility, followed by the condenser, the evaporator, and the expansion device.

## 6. ACKNOWLEDGEMENTS

The authors would like to acknowledge the financial support provided by FAPESC, under grant number 2021TR1481, and CNPq (Conselho Nacional de Desenvolvimento Científico e Tecnológico). Thanks, are also due to Mr. Jaime Fraga Freitas and Mr. Alberto Marques Hubener, from Karville (Joinville Comércio de Acessórios para Veículos), for their valuable contribution to the experimental work.

## 7. REFERENCES

ANFAVEA, 2023, Associação Nacional dos Fabricantes de Veículos Automotores, Brazilian Automotive Industry Yearbook 2023, São Paulo-SP, Brazil.

Bandarra Filho, E.P., Mendonza, O.S.H., 2010, Alternative Refrigerants to be used in air-conditioning systems in replace the R-134a, 13th Brazilian Congress of Thermal Sciences and Engineering.

Da Silva, D.L., Melo, C., 2016, A Perspective on R&D&I Activities in the Brazilian Mobile Air Conditioning Market, 16th Brazilian Congress of Thermal Sciences and Engineering, 2016, Vitoria-ES.

Da Silva, D.L., Cordova, G.M., 2017, Mathematical Model of an Automotive Air-Conditioning System under Steady-State Conditions. 24th ABCM International Congress of Mechanical Engineering (10.26678/ABCM.COBEM2017.COB17-0367).

Da Silva, D.L., Goedert, J., Hermes, C.J.L, Galvão, I., 2019, Evaluation of the thermal performance of forced condensers for bus air-conditioning systems. 25th International Congress of Mechanical Engineering (10.26678/ABCM.COBEM2019.COB2019-0522).

Caron, L.T., Hermes, C.J.L., Da Silva, D.L, 2022, Steady-state simulation of the air-conditioning system of a hybrid vehicle, 19th Brazilian Congress of Thermal Sciences and Engineering (10.26678/ABCM.ENCIT2022.CIT22-0260).

IEA, 2019, Cooling on the move, International Energy Agency.

Farrington R., Rugh J., 2000, Impact of Vehicle Air-Conditioning on Fuel Economy, Tailpipe Emissions, and Electric Vehicle Range, National Renewable Energy Laboratory.

Hermes, C.J.L, Boeng, J., Da Silva, D.L., Knabben, F.T., Sommers, A.D., Evaporator Frosting in Refrigerating Appliances: Fundamentals and Applications. Energies, v. 14, p. 5991, 2021.

Jabardo, J.M.S., Mamani, W.G., Ianella M.R., 2002, Modeling and experimental evaluation of an automotive air conditioning system with a variable capacity compressor, International Journal of Refrigeration, Vol. 25, pp. 1157–1172.

Johnson, V.H. 2002, Fuel used for vehicle air-conditioning: A state-by-state thermal comfort-based approach. SAE Technical Paper. 2002–01–1957.

Ko, J., Thu, K., Miyazaki, T., 2021. Transient analysis of an electric vehicle air-conditioning system using CO2 for start-up and cabin pull-down operations. Appl. Therm. Eng., v. 190, 116825.

Motor, 2022, Duster Oroch e Saveiro são os últimos carros sem ar-condicionado. Disponível em: https://motor1.uol.com.br/news/562155/dusteroroch-saveiro-sem-arcondicionado-brasil/. Accessed 12th May 2023.

Torregrosa-Jaime, B., Bjurling, F., Corberán J.M., Di Sciullo F, Payá, J., 2015, Transient thermal model of a vehicle's cabin validated under variable ambient conditions, Applied Thermal Engineering V. 75 pp. 45-53.

Kuwar Y.V., Narasimham G.S.V.L., 2020, Performance of Automotive Air Conditioning System with R134a and R1234yf, International Journal of Air-Conditioning and Refrigeration Vol. 28, No. 2 (2020) 2050013.

Unep, 2023, Kigali Amendment hits milestone 100th ratification, boosting climate action. United Nations Environment Programme, https://www.unep.org/news-and-stories/press-release/kigali-amendment-hits-milestone-100th-ratification-boosting-climate. Accessed 16th May 2023.

Wu, J., Zhou, G., Wang, M., 2020, A comprehensive assessment of refrigerants for cabin heating and cooling on electric vehicles, Applied Thermal Engineering 174, 115258.

Zhang, K., Li, M., Yang, C., Shao, Z., Wang, L. 2020. Exergy Analysis of Electric Vehicle Heat Pump Air Conditioning System with Battery Thermal Management System. J. Therm. Sci., v. 29, n.2, p. 408–422.

## 8. RESPONSIBILITY NOTICE

The authors are the only responsible for the printed material included in this paper.